Inverted Strip Dielectric Waveguide for Millimeter-Wave Integrated Circuits

TATSUO ITOH, SENIOR MEMBER, IEEE

Abstract—**A new type of dielectric waveguide, which has a number of advantages over other previously available waveguide structures for millimeter-wave integrated circuits, is described. Dispersion characteristics and the field distributions in the waveguide are calculated using the concept of effective dielectric constant. Field distributions have been measured in the 80-GHz range in order to check the accuracy of the analytical results. This measurement has been done using a novel experimental technique, which should also be applicable to many other millimeter-wave waveguides and components.**

I. Introduction

As the microwave integrated circuit technique is approaching its maturity, it is natural to investigate integrated circuits at millimeter-wave frequencies. Several types of waveguide structures are currently available for use in millimeter-wave integrated circuits: microstrip line [1], image guide [2], [3], silicon waveguide [4], etc. Recently, the author reported a novel waveguide called the strip dielectric guide (SDG) [Fig. 1(a)], in which the dielectric constant ε_2 of the guiding layer is chosen to be larger than those of the dielectric strip and the substrate, ε_1 and ε_3. Therefore, the electromagnetic energy is concentrated in the guiding layer immediately below the dielectric strip [5], [6]. The advantageous features of the waveguide are as follows.

1) When compared with conventional microstrip lines at millimeter frequencies, the size of the present waveguide is much larger. Typically, the thickness of each dielectric region as well as the width of the strip are of the order of the operating wavelength, e.g., 2–4 mm for 80-GHz operation, whereas the size of the microstrip line must be less than one-tenth of a wavelength. This larger size makes the mechanical fabrication much easier and more accurate; hence the production is much more economical.

2) Compared with image guides and other dielectric rod waveguides, the radiation loss due to surface roughness is smaller in the present structure, because in the SDG the dielectric strip is used to create a lens effect in the structure and the actual propagation takes place in the middle layer. It is relatively easy to construct a layered structure with extremely smooth surfaces. On the other hand, in other dielectric waveguides the energy propagates in the rod. Hence the surface roughness of its side walls enhances radiation losses. To minimize such losses, costly technological processes are needed to reduce the surface roughness.

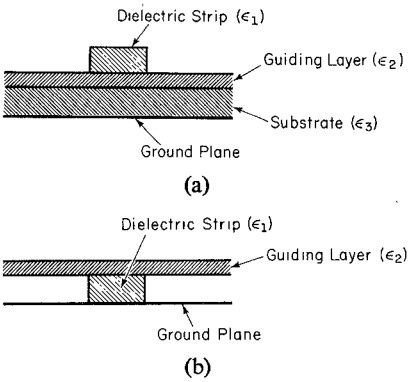

Fig. 1. Cross sections of new waveguide structures for millimeter-wave integrated circuits. (a) Strip dielectric waveguide. (b) Inverted strip dielectric waveguide.

3) The conductor loss in the ground plane is small since most of the energy is in the guiding layer. Yet the ground plane provides a heat sink and is convenient for dc biasing in solid-state device applications. Coupling of electromagnetic energy with such devices can be controlled by the geometry and the dielectric constant of the substrate material. In typical dielectric rod waveguides there is no ground plane. On the other hand, the ground plane in the image guide creates a substantial amount of conductor loss since the field is quite strong near the ground plane. Extreme care must be taken to reduce conductor loss in microstrip lines because the field is strong at the edges of the microstrip.

The inverted strip dielectric waveguide (ISG), which is the topic of this paper, is a natural extension of the SDG and operates on the same principle. As shown in Fig. 1(b), the ISG consists of a guiding layer with dielectric constant ε_2 placed on a dielectric strip ε_1 which in turn sits on a ground plane. Since $\varepsilon_1 < \varepsilon_2$, most of the electromagnetic energy is carried in the guiding layer immediately above the dielectric strip. In addition to the advantages of the SDG summarized previously, the ISG has even more attractive features.

4) Compared with the SDG, only two dielectric regions are involved. This may reduce the dielectric loss caused in the substrate in Fig. 1(a).

5) Bonding between two dielectric materials can be avoided. Once the dielectric strip is securely placed on the ground plane, the guiding layer is placed on top of it without the use of a bonding material at the interface of the two dielectric media. Instead, it is held securely by

Manuscript received August 1, 1975; revised September 9, 1975. This work was supported by the Joint Services Electronics Program (U.S. Army, U.S. Navy, U.S. Air Force) under Contract DAAB-07-72-C-0259.

The author was with the Coordinated Science Laboratory and the Department of Electrical Engineering, University of Illinois, Urbana, IL 61801. He is now with the Radio Physics Laboratory, Stanford Research Institute, Menlo Park, CA 94025.

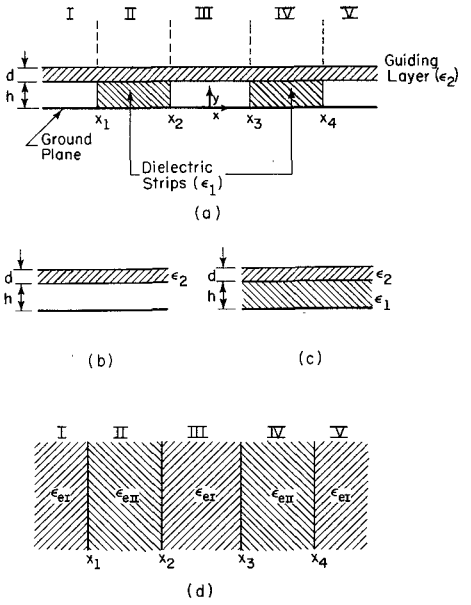

Fig. 2. (a) Coupled version of the ISG. (b) Structures for analyzing y variations in I, III, and V regions. (c) Structures for analyzing y variations in II and IV regions. (d) Structure for analyzing x variations using concept of effective dielectric constants.

the mechanical pressure between the guiding layer and the ground plane. The elimination of bonding material from the wave guiding region is useful from the point of view of reducing the propagation loss caused by the bonding material which is usually quite lossy, and further reduces the restriction on the choice of dielectric materials. Note that the strip can be bonded to the ground plane without significantly affecting the loss characteristic, because the field on the ground plane is small due to the nature of the waveguide.

However, in the design stages of millimeter-wave integrated circuits, the strips need not be bonded to the ground plane. In this way, the degree of coupling in the coupled guide [Fig. 2(a)] and between the guide and some lumped elements can be controlled by adjusting the relative location of each dielectric strip in the sideward direction. The strips will be bonded to the ground plane only after the adjustment is made.

The present analysis of ISG is based on the concept of effective dielectric constant [2], [3], [5], [6]. Numerical results are presented for dispersion characteristics and the field distributions in the ISG. The field distributions are measured in the 80-GHz range and the experimental data are compared with numerical results.

II. Method of Analysis

The ISG, which operates on the same physical principle as the SDG, will generally support two types of modal fields, classified as the $E_{pq}{}^{y}$ and $E_{pq}{}^{x}$ modes, where the subscripts p and q indicate the number of extrema of the electric field in the x and y directions, respectively. Since they are hybrid modes, it is possible to write fields of these modes in terms of two scalar potentials, ϕ^e and ϕ^h, which are proportional to the E_y and H_y fields.

$$E_y = \frac{1}{\varepsilon_r(y)}\left(k_z{}^2 - \frac{\partial^2}{\partial x^2}\right)\phi^e \tag{1}$$

$$H_y = \left(k_z{}^2 - \frac{\partial^2}{\partial x^2}\right)\phi^h \tag{2}$$

where $\varepsilon_r(y)$ is a relative dielectric constant in the region of the application and k_z is the propagation constant. Since both $E_{pq}{}^{y}$ and $E_{pq}{}^{x}$ modes can be analyzed in a similar manner, we will concern ourselves with only the $E_{pq}{}^{y}$ modes. Because the principal field components of $E_{pq}{}^{y}$ modes are E_y and H_x, ϕ^e has the dominant contribution and ϕ^h may be neglected if the width-to-thickness ratio of the strip is moderately large.

Under this assumption, we will derive the eigenvalue equation for the propagation constant k_z as well as the field distributions in the cross section of the general coupled-line structure shown in Fig. 2(a). Since the analysis is quite similar to the case of SDG's [5], [6], only the important steps will be summarized. Throughout the rest of the paper, we assume that both the dielectric materials and the conductor are lossless.

The analysis is based on the concept of effective dielectric constants originally developed by Toulios and Knox [3] and extended to the SDG by the present author [5], [6]. In Fig. 2(a), if each of regions I, II, III, IV, and V is taken to be infinitely long in the x direction, we have five slab waveguides. Regions I, III, and V have a single slab raised from the ground plane by a distance h [Fig. 2(b)], while regions II and IV are double-slab guides backed by the ground plane [Fig. 2(c)]. The propagation constants in both types of slab guides can be determined by matching the tangential electric and magnetic fields at each interface. Both of these structures can then be replaced by an equivalent infinite homogeneous region having some effective dielectric constants ε_{eII} (regions II and IV) and ε_{eI} (I, III, and V). The effective dielectric constant may be considered as that of a hypothetical medium in which the propagation constant is identical to the original structure.

The effective dielectric constant ε_{eII} may be obtained in the following manner. Assuming the traveling-wave solution inside the layer with highest dielectric constant (ε_2) and the decaying-wave expressions outside of this layer, one obtains the field distributions in the double-slab structure corresponding to regions II and IV [Fig. 2(c)] from

$$\phi^e(y) = \begin{cases} \cosh \eta_1 y, & 0 < y < h \\ \cosh \eta_1 h \cos [k_y(y-h)] & \\ \quad + \dfrac{\eta_1 \varepsilon_2}{k_y \varepsilon_1} \sinh \eta_1 h \sin [k_y(y-h)], & \\ & h < y < h + d \\ \cosh \eta_1 h \cos [k_y d] & \\ \quad + \dfrac{\eta_1 \varepsilon_2}{k_y \varepsilon_1} \sinh \eta_1 h \sin [k_y d] e^{-\eta_3(y-h-d)}, & \\ & y > h + d \end{cases} \tag{3}$$

where the normalization constant was omitted. Since (3) already incorporates the continuity of H_x at each interface, the eigenvalue equation is obtained by matching E_z at each interface

$$\eta_3\varepsilon_2 k_y\varepsilon_1 \cosh[\eta_1 h]\cos[k_y d] + \eta_3\varepsilon_2^2\eta_1 \sinh[\eta_1 h]\sin[k_y d] - k_y^2\varepsilon_1 \cosh[\eta_1 h]\sin[k_y d] + k_y\varepsilon_2\eta_1 \sinh[\eta_1 h]\cos[k_y d] = 0. \quad (4)$$

The quantities k_y, η_3, and η_1 are related via

$$k_0^2 + n_3^2 = \varepsilon_2 k_0^2 - k_y^2 = \varepsilon_1 k_0^2 + \eta_1^2 \quad (5)$$

where η_1 may be either real or imaginary, while k_y and η_3 always remain real.

The effective dielectric constant for this structure is

$$\varepsilon_{e\mathrm{II}} = \varepsilon_2 - \frac{k_y^2}{k_0^2}. \quad (6)$$

The corresponding quantity $\varepsilon_{e\mathrm{I}}$ for regions I, III, and V may be similarly derived.

Now coming back to the structure in Fig. 2(a), we replace regions I, III, V and II, IV by the hypothetical medium with the effective dielectric constants $\varepsilon_{e\mathrm{I}}$ and $\varepsilon_{e\mathrm{II}}$, respectively, even though each region is finite in extent in the x direction. The propagation constant k_z of the inverted dielectric guide is determined by matching the fields at each vertical interface of a five-layered structure shown in Fig. 2(d), which now models the original structure in Fig. 2(a).

If one writes $\phi^e(x)$ in appropriate forms in each layer and matches E_y and H_z fields at four interfaces, the eigenvalue equation for k_z is obtained:

$$k_z^2 = \varepsilon_{e\mathrm{II}}k_0^2 - k_x^2 = \varepsilon_{e\mathrm{I}}k_0^2 + \xi^2 \quad (7)$$

$$\{T_1\xi\cosh[\xi(x_3 - x_2)] - T_2 k_x \sinh[\xi(x_3 - x_2)]\}T_4 - \{T_2 k_x \cosh[\xi(x_3 - x_2)] - T_1\xi\sinh[\xi(x_3 - x_2)]\}T_3 = 0 \quad (8)$$

where

$$T_1 = \xi\sin[k_x(x_4 - x_3)] + k_x\cos[k_x(x_4 - x_3)]$$
$$T_2 = k_x\sin[k_x(x_4 - x_3)] - \xi\cos[k_x(x_4 - x_3)]$$
$$T_3 = \xi k_x\cos[k_x(x_2 - x_1)] + \xi^2\sin[k_x(x_2 - x_1)]$$
$$T_4 = -k_x^2\sin[k_x(x_2 - x_1)] + \xi k_x\cos[k_x(x_2 - x_1)].$$

The special case of the single line can be derived from the coupled-line analysis by letting $x_3 - x_2 = 2s \to \infty$ in (8):

$$(\xi^2 - k_x^2)\sin[k_x(x_2 - x_1)] + 2\xi k_x\cos[k_x(x_2 - x_1)] = 0. \quad (9)$$

Note that both k_x and ξ are real. Also when $x_2 - x_1 = x_4 - x_3 = 2w$, a certain symmetry can be used to simplify the problem. That is, either an electric or magnetic plane can be placed at $x = (x_2 + x_3)/2$, and corresponding to each case, even and odd modes can be obtained by one of two equations derivable from (8).

Before concluding this section, the numerical procedure should be summarized. First, (4) is solved numerically for k_y from which the effective dielectric constant $\varepsilon_{e\mathrm{II}}$ is obtained as defined in (6). The value of $\varepsilon_{e\mathrm{I}}$ is similarly obtained. Next, using these $\varepsilon_{e\mathrm{I}}$ and $\varepsilon_{e\mathrm{II}}$ values, (9) [or (8) for the coupled line] is solved for k_x. The propagation constant k_z is obtained from (7). The field distributions in the y direction in regions II and IV (not too close to the edges) may be obtained from (3) once k_y is determined. For the x direction, the field is obtained by substituting the k_x and ξ into appropriate expressions for $\phi^e(x)$.

It is possible that for a given frequency or k_0 both (4) and (8) [or (9)] have more than one solution. They give the higher order modes. To determine the specific orders p and q of the solutions, it is necessary to study both the eigenvalues of (4), (8), or (9) as well as the field distributions corresponding to the specific eigenvalue.

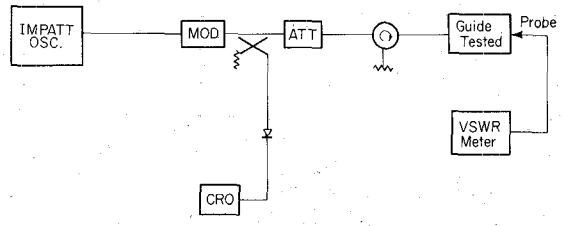

Fig. 3. Block diagram for field distribution measurements.

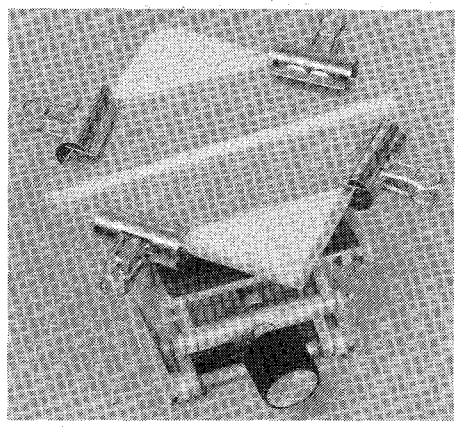

Fig. 4. Actual view of an ISG.

III. Experimental Procedure

In this section, a novel method for probing the field in the cross section of the ISG will be described. This technique is quite general and is applicable to detecting the field distributions in many other types of millimeter waveguides. The main purpose of the field measurement is to test the theoretical and numerical analysis. Since the measurement of dispersion characteristics requires a variable frequency source that was not available to the author, we have concerned ourselves only with the field measurements.

Fig. 3 shows a block diagram of the experimental setup. The millimeter-wave energy (81.7 GHz) is fed through the E-band waveguide system to the ISG and the field distributions are measured by the pinhole probe. The guide tested consists of a fused quartz plate (as a guiding layer) and a Teflon strip placed on an aluminum ground plane. One typical waveguide is shown in Fig. 4. Fig. 5 shows the

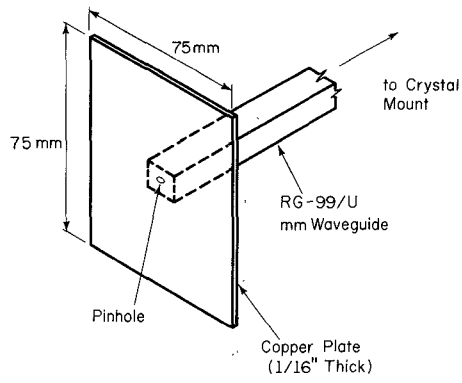

Fig. 5. Pinhole probe for field measurements.

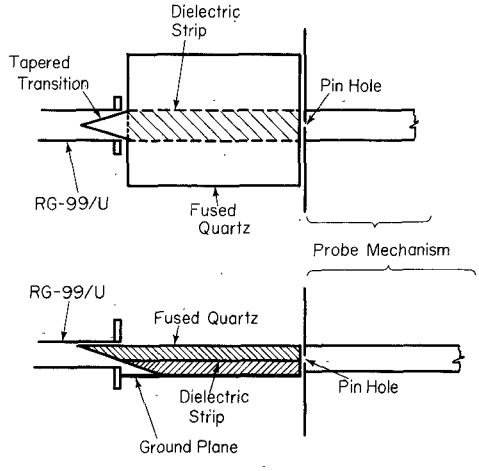

Fig. 6. Arrangement of the measurement setup.

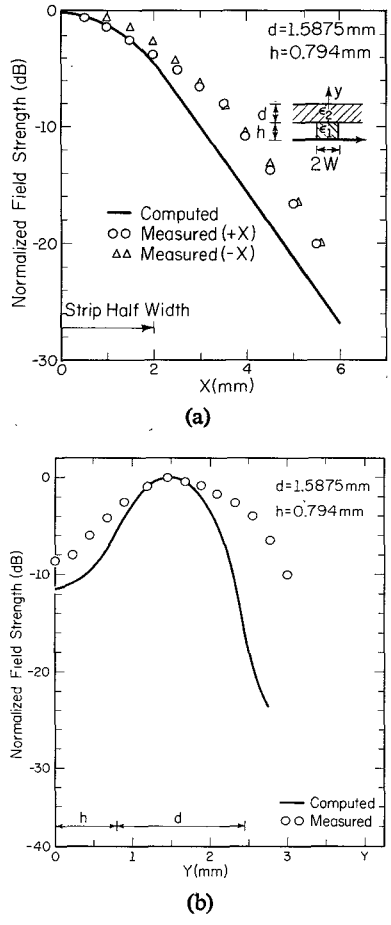

Fig. 7. Computed and measured field distributions at 81.7 GHz. $d = 1.5875$ mm, $h = 0.794$ mm, $w = 2$ mm, $\varepsilon_1 = 2.1$, and $\varepsilon_2 = 3.8$. (a) Sideward direction. (b) Vertical direction.

pinhole probe, which consists of a large copper plate welded to a standard RG-99/U open-ended waveguide, which is, in turn, connected to a crystal detector. A pinhole is drilled through the copper plate at the center of the rectangular waveguide. Fig. 6 depicts a detailed view of the tested waveguide and the probe section. The ISG has a tapered transition section to enhance the launching efficiency. The probe mechanism, including the crystal detector, is mounted on the three-axis vernier mechanism.

The measurement procedure is as follows. First, align the axis of the probe parallel to that of the ISG, while moving the probe close to the guide until the copper plate almost touches the open end of the guide. Now, the ISG is practically shorted, except for a small perturbation due to the pinhole. Hence the field distribution in the cross section of the guide is almost unaffected. Next, the field strength is recorded, while the probe is moved in the cross-sectional directions by two (x and y) vernier mechanisms. As long as the copper plate is large enough, these movements do not affect the field distributions in the guide cross section.

In the experiment, the $E_{11}{}^{y}$ mode has been excited, although there is a possibility that other modes could be excited at the transition junction; the experimental results revealed that only the dominant mode was present in the location of the probe.

IV. Results

Figs. 7–9 show the theoretical and experimental results for the field distributions in the cross sections of the ISG's. The width of the Teflon strip $2w$ and the thickness d of the guiding layer (fused quartz) are kept constant; each figure corresponds to the case of the different strip thickness h. From these figures, the agreement between the theoretical and experimental results, especially for the sideward (x) direction, is quite good. One of the reasons why the sideward direction cases give closer agreement may be that the field variation is slower in the sideward direction because the guide is quite thin in the vertical (y) direction. Hence the resolution of the probe detector is much better in this direction from the experimental point of view. It is possible to improve the resolution in the vertical direction by making the pinhole smaller; however, by doing so the power available to the crystal detector will be sacrificed and the dynamic range of the measurement will be reduced. The present data are the results of the compromise between the resolution and the dynamic range.

Note that good agreement in field distribution data with the measured results for various choices of cross-sectional parameters does not automatically guarantee that the present theory accurately predicts the dispersion characteristics. However, it implies that the propagation constants

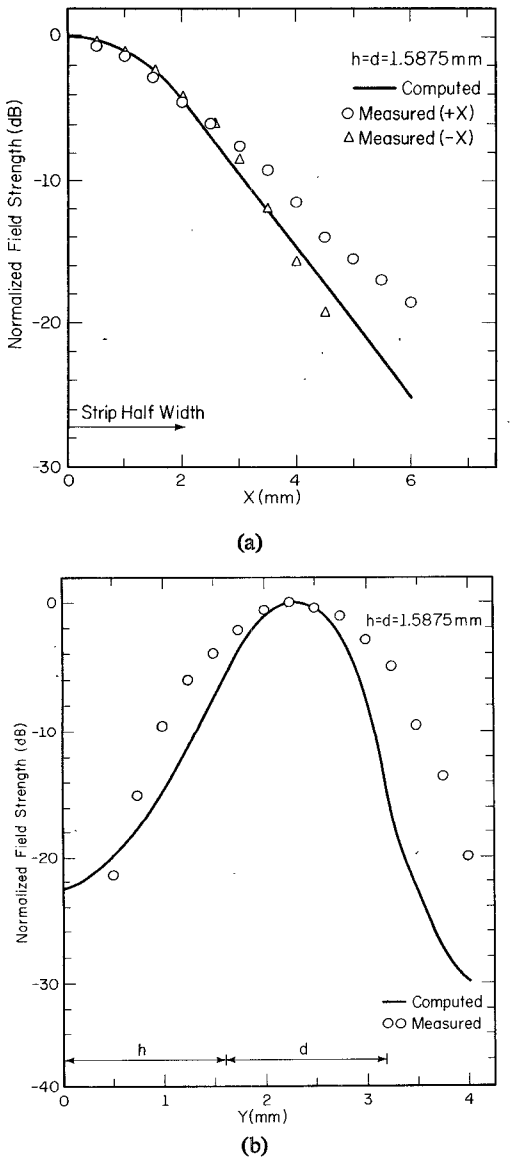

Fig. 8. Computed and measured field distributions at 81.7 GHz. $d = h = 1.5875$ mm, $w = 2$ mm, $\varepsilon_1 = 2.1$, and $\varepsilon_2 = 3.8$. (a) Sideward direction. (b) Vertical direction.

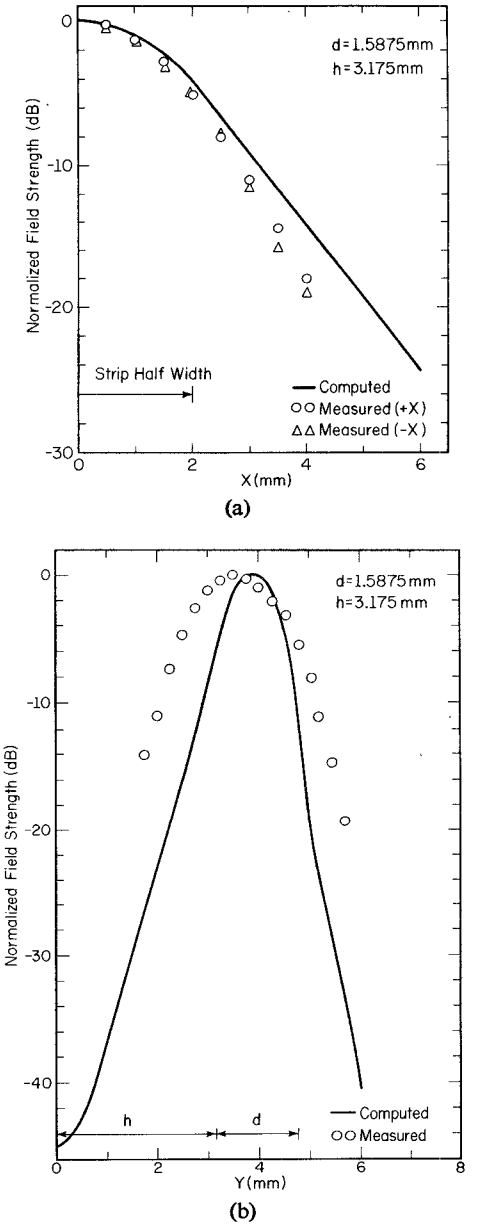

Fig. 9. Computed and measured field distributions at 81.7 GHz. $d = 1.5875$ mm, $h = 3.175$ mm, $w = 2$ mm, $\varepsilon_1 = 2.1$, and $\varepsilon_2 = 3.8$. (a) Sideward direction. (b) Vertical direction.

computed in the neighborhood of the frequency used are accurate. In fact, the field distributions were derived from the computed results of the propagation constants.

In Fig. 10 the strength of E_y at $x = 3w$ and some y, e.g., y_0, and that of H_x at $x = 0$ on the ground plane are shown versus the ratio of the strip thickness h to the guiding layer thickness d for several values of d. The strength of the E_y field is normalized by that of E_y at $x = 0$ (center of the guide) and $y = y_0$. These curves can be used as a measure of the guiding ability of the waveguide, because as the value decreases more energy is concentrated toward the center of the guide. Hence the values of h/d corresponding to the dips in the $|E_y|$ curves are the best choices when the guiding ability is the primary concern.

The magnitude of H_x at $x = 0$ and $y = 0$, that is, on the ground plane, is normalized by the maximum $|H_x|$ value at $x = 0$. Since H_x on the ground plane is proportional to the surface current J_z on the conductor, and since the conductor loss is proportional to the magnitude of J_z for a given conductivity, these curves for $|H_x|$ can be used as a measure of the conductor loss. Hence, for reducing the conductor loss, it is desirable to make the ratio h/d larger.

Fig. 11 shows the values of effective dielectric constants $\varepsilon_{e\mathrm{I}}$ and $\varepsilon_{e\mathrm{II}}$ and the normalized propagation constants k_z/k_0 versus the ratio h/d for two values of d. For small h/d, the changes of these values are rather quick. However, as h/d increases and hence the effect of the ground plane is reduced, k_z/k_0 as well as $\varepsilon_{e\mathrm{I}}$ and $\varepsilon_{e\mathrm{II}}$ approach some asymptotes. Hence a moderately large h/d might be chosen if one desires the change in thickness h due to temperature variation to exert little effect on the value of k_z/k_0.

From the results in Figs. 10 and 11, the best h/d ratio may be considered the compromise of various contrasting requirements. The guiding ability, the conductor loss, the effect

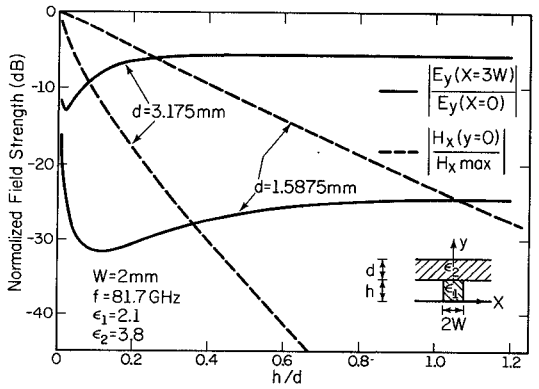

Fig. 10. Computed field strengths versus h/d.

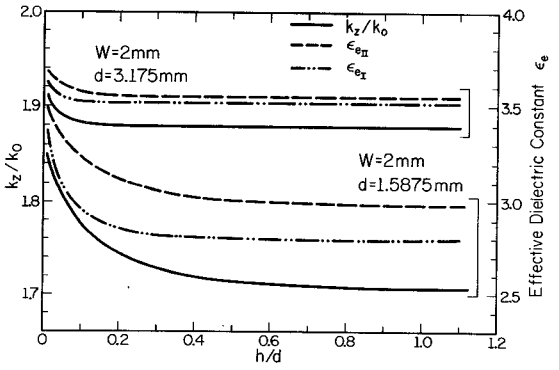

Fig. 11. Effective dielectric constants and the normalized propagation constant versus h/d at 81.7 GHz. $\varepsilon_1 = 2.1$ and $\varepsilon_2 = 3.8$.

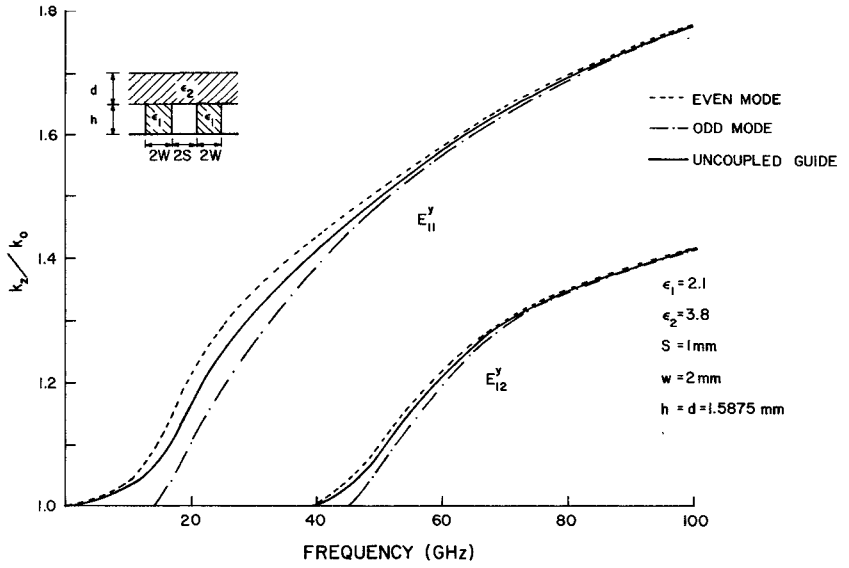

Fig. 12. Dispersion diagrams for coupled and uncoupled versions of the ISG.

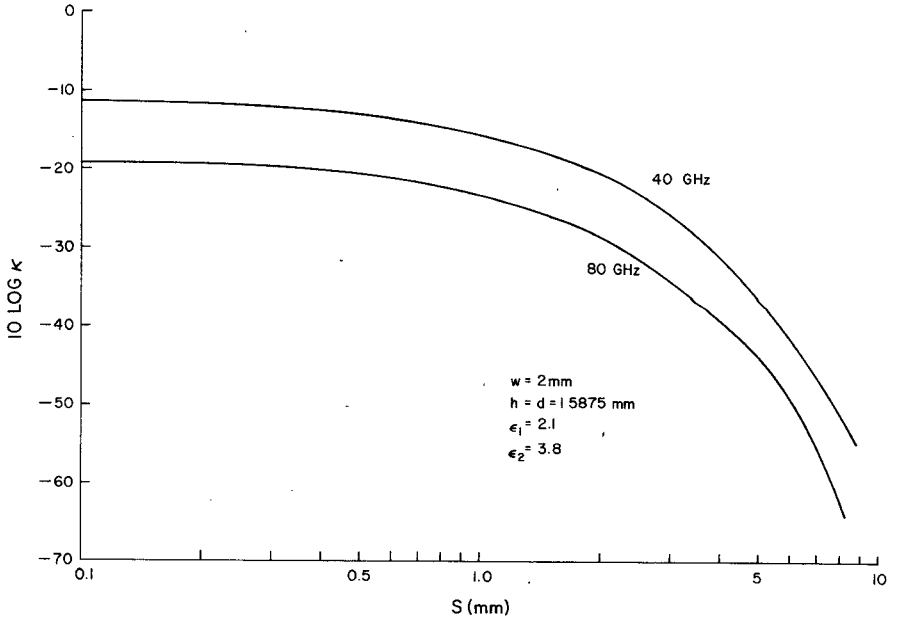

Fig. 13. Coupling factor κ versus half-separation s.

of temperature variation, etc., must be taken into consideration when one designs the ISG.

Fig. 12 presents dispersion characteristics of both single and coupled versions of the ISG with some typical parameters. The even and odd propagation constants approach the one for the uncoupled guide as the operating frequency gets higher. This phenomenon is due to the decrease of coupling between the two guides at the higher frequencies where the concentration of the fields in the regions above the strips becomes stronger.

Finally, Fig. 13 shows the coupling factor κ for the dominant even and odd modes versus the separation $2s$ of two guides. The parameter κ is defined as

$$\kappa = (k_{ze} - k_{zo})/k_z$$

where k_{ze} and k_{zo} are the propagation constants of the even and odd dominant $E_{11}{}^y$ modes in the coupled structure, while k_z is that of the $E_{11}{}^y$ mode in the uncoupled ($s = \infty$) guide.

V. Conclusion

In this paper, a novel waveguide structure, an ISG, has been analyzed both theoretically and experimentally. This waveguide is believed to be useful for millimeter-wave integrated circuits. Comparisons have been made, where feasible, between theoretical and experimental results and the agreement was found to be good. A number of numerical results useful for designing this type of waveguide are presented in addition to the dispersion diagrams.

Acknowledgment

The author wishes to thank the Fujitsu Laboratories, Kawasaki, Japan, for supplying an IMPATT oscillator and several other millimeter-wave components. He also wishes to thank Dr. T. Rozzi of the University of Illinois, on leave from Phillips Laboratories, The Netherlands, for reading the manuscript.

References

[1] M. V. Schneider, "Millimeter-wave integrated circuits," in *International Microwave Symposium Digest*, pp. 16–18, (Chicago, Illinois, June 4–6, 1973).
[2] R. M. Knox and P. P. Toulios, "A *V*-band receiver using image line integrated circuits," in *Proceedings of the National Electronics Conference*, vol. 29, pp. 489–492, Oct. 16–18, 1974.
[3] P. P. Toulios and R. M. Knox, "Image line integrated circuits for system applications at millimeter wavelengths," U.S. Army Electronics Command, Final Report, Rept. No. ECOM-73-0217-F, July 1974.
[4] H. Jacobs and M. M. Chrepta, "Electronic phase shifter for millimeter-wave semiconductor dielectric integrated circuits," *IEEE Trans. Microwave Theory Tech.*, vol. MTT-22, no. 4, pp. 411–417, April 1974.
[5] T. Itoh and R. Mittra, "New waveguide structures for millimeter-wave integrated circuits," in *International Microwave Symposium Digest*, pp. 277–279, Palo Alto, CA, May 12–14, 1975.
[6] W. McLevige, T. Itoh, and R. Mittra, "New waveguide structures for millimeter wave and optical integrated circuits," *IEEE Trans. Microwave Theory Tech.*, vol. MTT-23, no. 10, Oct. 1975.

Double-Layered Slot Line for Millimeter-Wave Integrated Circuits

NIKOLA SAMARDZIJA AND TATSUO ITOH, SENIOR MEMBER, IEEE

***Abstract*—A new type of waveguide, a double-layered slot line, is described which is useful for millimeter-wave integrated circuits (IC's). Galerkin's method applied in the Fourier transform domain is used for analyzing the propagation characteristics of the dominant mode in the structure. Theoretical and experimental results are presented and compared.**

Manuscript received January 19, 1976; revised May 4, 1976. This work was supported in part by the Joint Services Electronics Program (U.S. Army, U.S. Navy, U.S. Air Force) under Contract DAAB-07-72-C-0259, and in part by the U.S. Army Research Office under Contract DAHCO4-74-G-0113. Part of this paper was presented at the IEEE International Microwave Symposium, Palo Alto, CA, May 12–14, 1975.

N. Samardzija was with the Coordinated Sciences Laboratory and the Department of Electrical Engineering, University of Illinois, Urbana, IL 61801. He is now with the Department of Electrical Engineering, Couren College of Engineering, University of Houston, Houston, TX 77004.

T. Itoh was with the Coordinated Sciences Laboratory and the Department of Electrical Engineering, University of Illinois, Urbana, IL 61801. He is now with the Radio Physics Laboratory, Stanford Research Institute, Menlo Park, CA 94025.

I. Introduction

RECENTLY, considerable interest has been shown for the millimeter-wave integrated circuits (IC's) for use in radiometry, radar, astronomy, and communications. Several types of waveguides convenient for millimeter-wave IC applications have been proposed. They include microstrip line [1], image guide [2], silicon guide [3], and strip dielectric guide [4].

At millimeter-wave frequencies the microstrip line shows a considerable conductor loss, and its dimensions are so small that the fabrication requires sophisticated technology. In the case of the image guide, the conductor loss is also a problem since the fields are quite strong on the ground plane. In the strip dielectric guide, the main flow of the electromagnetic waves lies in the dielectric layer away from the ground plane. Hence the loss is reduced considerably [4].